Int. J. Heat Mass Transfer. Vol. 23, pp. 1137–1146.

0017-9310/80/0801-1137 $02.00/0

CONVECTIVE–RADIATIVE INTERACTION IN A PARALLEL PLATE CHANNEL—APPLICATION TO AIR-OPERATED SOLAR COLLECTORS

C. H. LIU* and E. M. SPARROW
Department of Mechanical Engineering, University of Minnesota, Minneapolis, MN 55455, U.S.A.

(*Received* 18 *December* 1979 *and in revised form* 12 *February* 1980)

Abstract—An analysis is made for simultaneously developing laminar velocity and temperature fields in a parallel plate channel in which convective and radiative heat transfer interact. One wall of the channel is externally heated and the other is externally insulated; air is the heat transfer fluid. These conditions are similar to those in an air-operated flat-plate solar collector. The results show that the radiant interchange causes the task of convective heating of the fluid to be shared between the two walls, with as much as 40% of the convective transfer taking place at the externally adiabatic wall. This can give rise to a significant reduction of the temperature of the directly heated wall which, for a solar collector, tends to improve its efficiency. The Nusselt numbers in the presence of radiation are higher than those for pure forced convection.

NOMENCLATURE

A, surface area;
F, angle factor;
H, channel height;
h, local heat transfer coefficient, $q_c/(T_w - T_b)$;
k, thermal conductivity;
L, channel length;
Nu, local Nusselt number on heated wall, $h(2H)/k$;
P, dimensionless pressure, equation (2);
p, pressure;
Pr, Prandtl number;
q_c, local convective heat flux;
q_r, local radiative heat flux;
q_w, local external heat flux;
Re, Reynolds number, $\bar{u}(2H)/\nu$;
T, absolute temperature;
T_b, bulk temperature;
T_w, wall temperature;
T_I, inlet-plenum and fluid inlet temperature;
T_{II}, exit-plenum temperature;
X, Y, dimensionless coordinates, equation (1);
x, y, physical coordinates, Fig. 1;
U, V, dimensionless velocities, equation (1);
u, v, velocity components;
$\bar{u}$, mean velocity;
η, x-coordinate along heated wall;
θ, dimensionless temperature, T/T_I;
ν, kinematic viscosity;
ξ, x-coordinate along unheated wall;
σ, Stefan–Boltzmann constant.

* Present address: Owens-Corning Technical Center, Granville, Ohio, U.S.A.

INTRODUCTION

IN RECENT years, there has been a number of studies of the interaction between forced convection and radiation heat transfer in pipes and ducts. In the main, these studies have been concerned with flowing fluids which participate in the radiation process, although some of the earlier work dealt with radiatively nonparticipating fluids. Air may be regarded as a radiatively nonparticipating fluid, and when air flows under laminar conditions the relatively low convective heat transfer coefficients provide a setting for significant effects of radiative transfer between the duct walls. This paper deals with one such situation, namely, laminar flow of air in a parallel plate channel which is uniformly heated at one wall and adiabatic at the other. A schematic diagram of the physical situation is shown in Fig. 1.

The present work was initially motivated by flat

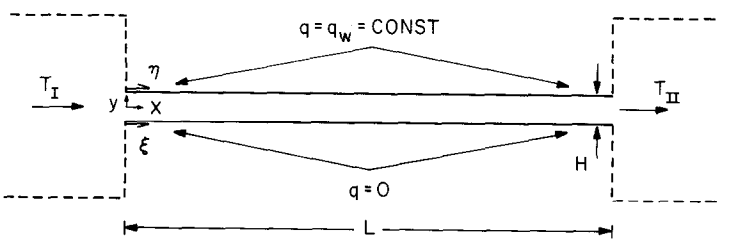

FIG. 1. Schematic diagram of the parallel plate channel.

plate solar collectors in which air is employed as the transfer fluid. Although the analysis and results are not limited to solar collector applications, it is edifying to discuss air-operated collectors in order to show the basis of the present analytical model.

In the standard type of air-operated solar collector presently in use today, the solar flux absorbed by the collector plate is transferred to an air stream which passes through a flat rectangular duct of large cross-sectional aspect ratio. The duct is situated immediately beneath the collector plate, so that the plate serves as the upper wall of the duct. The lower wall of the duct is an insulated surface. Typically, the height H of the duct is 1 cm (0.394 in.) and its length L (per collector panel) is 1.98 m ($6\frac{1}{2}$ ft). The rate of airflow through the duct is usually selected to be 2 ft^3/min per square foot of collector surface [1]. The corresponding Reynolds number (based on an equivalent diameter $D_e = 2H$) is about 2300.

With regard to flow regimes (i.e. laminar vs turbulent) in a parallel plate channel, an extensive experimental study [2] encompassing 12 entrance and disturbance configurations indicated that laminar flow commonly persisted up to $Re = 2600$ or greater if the sources of disturbance are not situated within the channel proper. In view of this and of the aforementioned value of 2300, there is a basis for considering a laminar flow model in the analysis of the heat transfer processes taking place in the collector airflow passages. There are, of course, other operating conditions (e.g., a series arrangement of collector panels) where higher Reynolds numbers will be encountered. These cases may be characterized by transitional flows (i.e. intermittently turbulent), so that a model based on fully turbulent conditions is inappropriate. For these transitional cases, the results of a laminar flow analysis may have trendwise relevance.

The analysis to be performed here will be concerned with high Reynolds number laminar flows ($Re = 1500$–2500). At these Reynolds numbers, there is a long hydrodynamic development length ($\sim 100H$ at $Re = 2500$). Therefore, in the analysis, account will be taken of the simultaneous development of the velocity and temperature distributions along the length of the channel.

The presence of radiative transfer is expected to improve the efficiency with which heat is transferred from the heated plate to the fluid, i.e. it should lower the temperature of the heated plate. This expectation is based on the belief that radiation will deliver energy to the otherwise unheated plate (lower plate of Fig. 1) which, in turn, will transfer heat to the fluid by convection. Thus, radiation serves as an enhancement mechanism. The maximum effect of the radiative transfer will occur when the surfaces of the channel are black, and it is, therefore, natural to focus attention on the black case, as has been done here.

The starting point of the analysis is the governing differential equations expressing conservation of mass, momentum and energy for the fluid, supplemented by the radiative transfer equations for the walls. This complex system does not admit an analytical solution, and numerical techniques were employed. The problem is governed by five parameters, so that care has to be exercised in the selection of cases for which solutions are obtained, especially since each case yields presentable results for the temperatures and heat fluxes at the heated and unheated walls, the bulk temperature, and the Nusselt number. The approach finally chosen was to define a base case (typical of solar collector operation) and then to systematically change the parameter values relative to those of the base case.

A literature search yielded two papers which, although having a filial relationship to the present work, are distinctly different. In [3], consideration was given to the interaction of radiation and convection in a parallel plate channel, but the task of solving the convection problem was avoided by assuming that the heat transfer coefficients were known. Such an approach is not applicable in the present problem because the coefficients are not known beforehand but depend on the temperature distributions along the walls (which are found from the solutions). In [4], the task of solving the convection problem was also avoided—in that case by making use of series solutions for hydrodynamically developed laminar channel flow with uniform wall heat flux. That method is also inapplicable to the present problem but, even if it were, its use would have involved greater complexity and yet would have provided results of lesser accuracy than the present direct solution method.

ANALYSIS

Formulation of the governing equations

To prepare the governing equations for solution, dimensionless variables and parameters are first introduced as follows

$$X = x/H, \quad Y = y/H, \quad U = u/\bar{u}, \quad V = v/\bar{u} \tag{1}$$

$$P = p/\rho\bar{u}^2, \quad \theta = T/T_1, \quad Re = \bar{u}(2H)/\nu \tag{2}$$

where all temperatures are expressed in absolute units. With these, the mass, momentum and energy equations for the fluid are expressible as

$$\frac{\partial U}{\partial X} + \frac{\partial V}{\partial Y} = 0 \tag{3}$$

$$U\frac{\partial U}{\partial X} + V\frac{\partial U}{\partial Y} = -\frac{\mathrm{d}P}{\mathrm{d}X} + \frac{2}{Re}\frac{\partial^2 U}{\partial Y^2} \tag{4}$$

$$U\frac{\partial \theta}{\partial X} + V\frac{\partial \theta}{\partial Y} = \frac{2}{RePr}\frac{\partial^2 \theta}{\partial Y^2}. \tag{5}$$

In these equations, the streamwise second derivatives have been omitted, as have cross sectional pressure variations; in addition, the y-momentum equation has been suppressed altogether. Such a model (which is actually a boundary layer model) is altogether valid for high laminar Reynolds numbers, as are being considered here.

It may also be noted that equations (3) and (4)

contain three unknowns, U, V and P. An additional equation, needed to make the system determinate (actually, to determine P), is obtained from the condition that the same mass flow passes through all cross sections of the channel.

The foregoing equations are the conventional equations for hydrodynamically and thermally developing duct flows. They may be supplemented by the wall and inlet conditions for the velocity. At the wall, no-slip and impermeability give, respectively,

$$U = V = 0, \tag{6}$$

while for a flat velocity profile at the inlet

$$U = 1, \qquad V = 0. \tag{7}$$

The special features of the problem arise through the thermal boundary conditions, which couple the convection to the radiation. For concreteness, the thermal boundary condition at the externally heated wall (upper wall of Fig. 1) will be dealt with first, after which the boundary condition at the externally adiabatic wall (lower wall) will be written. If q_c and q_r denote the local convective and radiative fluxes leaving a position $X = \eta$ on the heated wall, then

$$q_c(\eta) + q_r(\eta) = q_w = \text{constant}. \tag{8}$$

The convective flux follows directly from Fourier's law as

$$q_c(\eta) = (kT_I/H)(\partial\theta/\partial Y). \tag{9}$$

The radiative flux requires a more comprehensive treatment, as will now be outlined.

The radiative flux q_r at surface location η is the net of the emitted radiation and the absorbed radiation at that location. For a black surface, the radiation emitted at η per unit time and area is $\sigma T^4(\eta)$, while the absorbed radiation is identically equal to the incident radiation. The incident radiation arriving at η comes from three zones: (i) the opposite wall, (ii) the channel inlet aperture at $X = 0$, and (iii) the channel exit aperture at $X = L/H$. The radiation entering the channel via the apertures, i.e. (ii) and (iii), may have a variety of characteristics depending on the nature of the upstream and downstream plenums. For generality, the respective plenums will be regarded as isothermal zones with temperatures T_I and T_{II}.

The mathematical representation of the incident fluxes (i), (ii) and (iii) will be dealt with only briefly here since similar descriptions are available elsewhere (e.g., [5], Chapter 3). With regard to (i), it may be noted that the black-body radiation emitted at a position ξ on the opposite wall is $\sigma T^4(\xi)\mathrm{d}A_\xi$, of which a fraction $\mathrm{d}F_{\xi-\eta}$ arrives at η (the factor F is termed an angle factor). The reciprocity rule for angle factors states that $\mathrm{d}A_\xi\,\mathrm{d}F_{\xi-\eta} = \mathrm{d}A_\eta\,\mathrm{d}F_{\eta-\xi}$. Therefore, the radiation emitted at ξ which arrives per unit area at η is $\sigma T^4(\xi)\mathrm{d}F_{\eta-\xi}$. Contributions of this type are delivered to η from all points between $\xi = 0$ and $\xi = L/H$, and the total is obtained by integration.

For (ii), the assumption of an isothermal plenum at temperature T_I means that the radiation streaming into the channel through the inlet aperture (area A_I) is $\sigma T_I^4 A_I$, of which a fraction $\mathrm{d}F_{I-\eta}$ arrives at η. The application of the reciprocity rule $A_I\,\mathrm{d}F_{I-\eta} = \mathrm{d}A_\eta F_{\eta-I}$ then gives that $\sigma T_I^4 F_{\eta-I}$ arrives per unit area at η. A similar development shows that $\sigma T_{II}^4 F_{\eta-II}$ arrives at η from the exit aperture.

It is now possible to bring together all that has been developed between equation (8) and the present. When dimensionless variables are introduced, there follows

$$\frac{\partial\theta}{\partial Y} = \frac{q_w H}{T_I k} - \frac{\sigma T_I^3}{(k/H)}\left[\theta^4(\eta) - \int_{\xi=0}^{L/H}\theta^4(\xi)\mathrm{d}F_{\eta-\xi} - F_{\eta-I} - \theta_{II}^4 F_{\eta-II}\right]. \tag{10}$$

Equation (10) expresses the derivative $\partial\theta/\partial Y$ at a point η on the heated (i.e. upper) wall in terms of the temperature at η, of the temperatures at all points ξ on the externally adiabatic wall, and of the temperature in the downstream plenum. If the right-hand side of equation (10) were known, as, for example, from a preceding cycle of an iterative solution method, then the value of $\partial\theta/\partial Y$ could be regarded as known. Such known values of $\partial\theta/\partial Y$ at all $0 \le \eta \le L/H$ could then serve as the boundary condition for the convective energy equation (5).

To determine a corresponding boundary condition for the externally adiabatic wall, an analysis similar to the foregoing is made, with the end result

$$-\frac{\partial\theta}{\partial Y} = \frac{\sigma T_I^3}{(k/H)}\left[-\theta^4(\xi) + \int_{\eta=0}^{L/H}\theta^4(\eta)\mathrm{d}F_{\xi-\eta} + F_{\xi-I} + \theta_{II}^4 F_{\xi-II}\right]. \tag{11}$$

Again, if the right-hand side were tentatively known at all $0 \le \xi \le L/H$, this equation can be employed as a boundary condition for the solution of the convection problem.

It may be noted that equations (10) and (11) contain two parameters

$$\frac{\sigma T_I^3}{(k/H)}, \qquad \frac{q_w H}{T_I K} = \frac{q_w}{\sigma T_I^4}\,\frac{\sigma T_I^3}{(k/H)}. \tag{12}$$

The first of these can be regarded as a measure of the relative strengths of the radiative and convective transport modes. The second has been rephrased in equation (12) to form the group $q_w/\sigma T_I^4$, which will be regarded here as an index of the strength of the external heating.

It is also interesting to identify the message of equations (10) and (11) with regard to convective heat transfer. In (10), the quantity $\partial\theta/\partial Y$ represents, in a nondimensional form, the local convective heat transfer from locations on the heated wall to the fluid. In the absence of radiation, the uniform heat flux boundary condition corresponds to $\partial\theta/\partial Y = q_w H/T_I k$. The radiation term appearing in (10), contained within the square brackets, is expected to be positive. Therefore,

the expected effect of radiation is to reduce the convective heat transfer at the heated wall of the channel.

In equation (11), the quantity $(-\partial\theta/\partial Y)$ denotes the local convective flux from a point ξ on the unheated wall to the fluid. In the bracketed term on the right of (11), the absorbed radiation is expected to exceed the emitted radiation, which results in a positive value of the convective heat flux. The foregoing observations, taken together, indicate that the main role of the radiation is to shift some of the burden of the convective heat transfer from the heated to the unheated wall.

To complete the specification of the problem, it remains to deal with the temperatures at the inlet and exit of the duct. The convection problem only requires that the inlet temperature be given, and the condition $T = T_1$ yields

$$\theta = \theta_1 = 1 \qquad \text{at} \quad X = 0. \tag{13}$$

The radiation problem requires values of the temperatures in both the inlet and exit plenums. Depending on the geometrical configurations of the plenums, it is conceivable that the temperature of the plenum walls will not equal that of the fluid in the respective plenum. The deviations will depend on the specifics of the particular situation. For a general study, such as that performed here, it appears appropriate to take the wall and fluid temperatures in each plenum to be equal. Thus, for the radiation problem,

$$\theta = \theta_1 = 1 \qquad \text{at} \quad X = 0 \tag{14}$$

$$\theta = \theta_{II} = \text{fluid bulk temperature} \qquad \text{at} \quad X = L/H. \tag{15}$$

A final aspect of the specification of the problem is to provide expressions for the angle factors that appear in equations (10) and (11). This information will be conveyed shortly when the solution methodology is described.

Solution methodology

The governing equations that were presented in the prior section of the paper were solved numerically by finite difference procedures. A general outline of the solution scheme will be discussed first, with details to follow. For a given Reynolds number Re and channel length L/H, a solution was first obtained for the velocity problem defined by equations (3), (4), (6) and (7). Then, attention was turned to the heat transfer problem and, to define a given case, numerical values were assigned to $\sigma T_1^3/(k/H)$, $q_w/\sigma T_1^4$, and Pr, with $q_w H/T_1 k$ being determined from the product of the first two of these. A solution was first obtained for the pure convection case: that is, the energy equation (5) was solved subject to radiation-free forms of equations (10) and (11) and to equation (13). Then, the pure convection solution was employed to initiate an iterative scheme for solving the coupled radiation-convection problem.

From the pure convection solution, temperature distributions $\theta(\eta)$ and $\theta(\xi)$, respectively corresponding to the heated and unheated walls, are available, as is the fluid bulk temperature at the channel exit [equal to θ_{II} according to equation (15)]. With these inputs, the right-hand sides of equations (10) and (11) can be evaluated, and this yields the distributions of $\partial\theta/\partial Y$ along the heated and unheated walls. These boundary conditions, together with $\theta = 1$ at $X = 0$, may then be employed for the solution of the energy equation (5), and this solution yields new values for $\theta(\eta)$, $\theta(\xi)$, and θ_{II}. Equations (10) and (11) can then be re-evaluated and equation (5) solved anew. This procedure was continued to convergence, which usually occurred within five cycles of iteration.

The finite difference methodology used for the velocity problem and for the convective part of the heat transfer problem is an adaptation of the Patankar—Spalding boundary layer procedure [6]. That procedure was modified in accordance with the appendix of [7] to facilitate the determination of the unknown pressure gradient dP/dX that appears in equation (4). To obtain highly accurate solutions, approximately 5700 grid points were deployed throughout the flow field—30 points in each of 187 cross sections. To accommodate the larger gradients, the points were more densely positioned near the channel walls. A higher concentration of points was also employed at small and moderate X values to adapt to the velocity and thermal development; the grid was also refined near $X = L/H$ to accommodate rapid temperature changes induced by radiation transfer to the downstream plenum.

The integral terms of equations (10) and (11) (associated with the radiation streaming between the walls) were also recast in finite difference form. In this connection, let $(\xi_2 - \xi_1)$, $(\xi_3 - \xi_2)$, ..., $(\xi_N - \xi_{N-1})$ represent the lengths of successive line segments deployed along the unheated wall. Furthermore, let $\gamma_i = (\xi_i + \xi_{i+1})/2$ denote the midpoints of the segments. Similarly, the heated wall is envisioned as being made up of segments of length $(\eta_{n+1} - \eta_n)$ with midpoint $\psi_n = (\eta_n + \eta_{n+1})/2$. Then, with these, the integral term of equation (10) was represented as

$$\sum_{i=1}^{N-1} \theta^4(\gamma_i) F_{\psi_n - \gamma_i} \tag{16}$$

where the angle factor relates to interchange between segments of length $(\eta_{n+1} - \eta_n)$ and $(\xi_{i+1} - \xi_i)$, respectively situated on the heated and unheated walls. The angle factor was evaluated using equation (4–65) of [5], with the result

$$\begin{aligned} 2(\eta_{n+1} - \eta_n) F_{\psi_n - \gamma_i} = {} & [(\eta_{n+1} - \xi_i)^2 + 1]^{1/2} \\ & + [(\eta_n - \xi_{i+1})^2 + 1]^{1/2} \\ & - [(\eta_{n+1} - \xi_{i+1})^2 + 1]^{1/2} \\ & - [(\eta_n - \xi_i)^2 + 1]^{1/2}. \end{aligned} \tag{17}$$

A similar approach was employed for evaluating the integral term of equation (11). The angle factors $F_{\eta_n - \gamma_i}$,

$F_{\eta-\mathrm{II}}$, etc. were evaluated for exchange between the segment $(\eta_{n+1}-\eta_n)$ and the aperture areas A_{I} and A_{II}.

Since the two walls were subdivided into identical distributions of line segments, the angle factor matrix is symmetric. It can, therefore, be stored in a one-dimensional array following the sequence (1,1), (2,1), (2,2), (3,1), (3,2), (3,3), (4,1), ... The angle factors were calculated once (via double precision) and retrieved when needed according to the aforementioned indexing sequence.

RESULTS AND DISCUSSION

Although the heat transfer coefficient h (or Nusselt number) is traditionally the main focus in a presentation of results, there are good reasons for not giving it top billing here. The essential fact is that due to the action of radiation, the local convective heat transfer q_c, the local wall temperature T_w and the local bulk temperature T_b are all unknown functions of x. Since these quantities are, in fact, the ingredients that comprise the heat transfer coefficient, it follows that giving numerical values of h is equivalent to giving a relationship between three unknowns. In view of this, it is appropriate to explicitly present results for q_c, T_w and T_b, all as functions of x. Furthermore, in the presentation, account has to be taken of the fact that the values of q_c and T_w on the heated wall are different from those on the unheated wall. For completeness, Nusselt number results are also given.

For a dimensionless presentation, the local heat transfer results are expressed as q_c/q_w which, in terms of the variables of the analysis, was evaluated from

$$q_c/q_w = \pm(\partial\theta/\partial Y)/(q_w H/T_{\mathrm{I}} k). \tag{18}$$

In this equation, the plus sign is used with $\partial\theta/\partial Y$ on the heated wall and the minus sign is taken with $\partial\theta/\partial Y$ on the unheated wall.

The wall and bulk temperatures are reported in ratio form, namely $\theta_w = T_w/T_{\mathrm{I}}$ and $\theta_b = T_b/T_{\mathrm{I}}$, where

$$\theta_b = \int \theta U \,\mathrm{d}Y \Big/ \int U \,\mathrm{d}Y \tag{19}$$

with the integrals extending over the range $0 \le Y \le 1$. Local Nusselt numbers were evaluated only at the heated wall according to the definition

$$Nu = \frac{q_c}{T_w - T_b}\frac{2H}{k} = \frac{2(\partial\theta/\partial Y)}{\theta_w - \theta_b}. \tag{20}$$

In planning the presentation of results, account has to be taken of the fact that there are five independent parameters, Re, Pr, L/H, $\sigma T_{\mathrm{I}}^3/(k/H)$ and $q_w/\sigma T_{\mathrm{I}}^4$. Furthermore, for each case, the distributions of T_w, T_b, q_c, and Nu are to be plotted as a function of x. Clearly, a conventional parametric study is precluded because space would not be available to present the avalanche of results that would be forthcoming. The approach adopted to deal with this situation was to select a base case (typical of solar collector operation) and then to examine the trends in the results as the parameters are changed relative to the base-case values. The base case

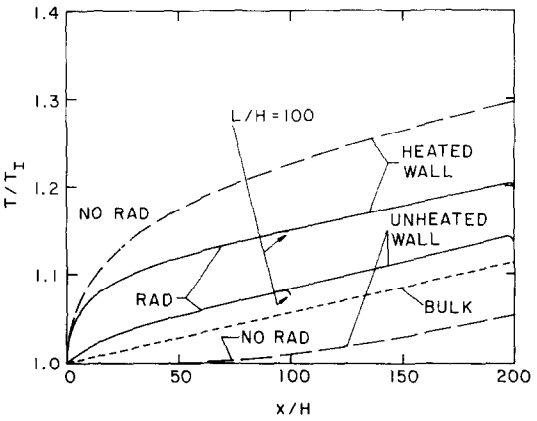

FIG. 2. Wall and bulk temperature distributions for the base case [equation (21)] and for a variant with $L/H = 100$.

was specified as follows

$$Re = 2500, \quad Pr = 0.7, \quad L/H = 200,$$
$$\sigma T_{\mathrm{I}}^3/(k/H) = 0.5, \quad q_w/\sigma T_{\mathrm{I}}^4 = 1. \tag{21}$$

For all of the other cases, the Prandtl number was maintained at a value of 0.7.

Wall and bulk temperature distributions

The base-case wall and bulk temperatures are plotted as a function of position along the length of the channel in Fig. 2, where it should be noted that all temperatures are expressed in absolute units. In addition to the results which include the effect of radiative transfer, the figure also contains results corresponding to pure forced convection (i.e. radiation suppressed altogether). The comparison between the results with and without radiative participation is of importance for two reasons. First, prior to the present investigation, the pure convection results would have been employed to calculate system heat transfer performance, without any assessment of the radiation effect. Therefore, the comparison reveals the errors inherent in neglecting radiation. Second, the comparison shows the degree of heat transfer enhancement, as reflected by a reduction in the temperature of the heated wall, that occurs due to radiation.

Examination of the figure reveals that whereas all temperatures increase with x as expected, there are significant differences between the results with and without radiation. At the heated wall, the rate of increase of the temperature with x is substantially smaller with radiation than without, resulting in a significant reduction in the wall temperature at downstream locations. Thus, for example, in a solar collector application in which $T_{\mathrm{I}} = 70°\mathrm{F} \simeq 530°\mathrm{R}$, there may be wall temperature reductions of 50°F at the specified operating conditions [equation (21)]. Even greater reductions will occur at higher values of $q_w/\sigma T_{\mathrm{I}}^4$ which may sometimes be encountered in solar applications.

For a solar collector, the practical effect of a reduction of the temperature of the heated wall is a

decrease of the heat loss from that wall [i.e. from the collector plate through the cover plate(s) to the environment]. Such a decrease in heat losses brings about an increase in the efficiency of the collector. Therefore, the radiative transfer between the walls of the airflow passage appears to have an affirmative effect on the performance of the collector.

This conclusion is somewhat tempered by another characteristic that may be observed in Fig. 2, namely, that the temperature of the unheated wall is substantially elevated by the effect of radiation. Such an elevation tends to increase the heat loss from the rear side of the collector. However, it is much easier to defend against rear-side losses (by an insulation layer) than against losses that take place through the cover plates. Therefore, the radiation-induced reduction in losses due to a decrease in the temperature of the collector plate (i.e. the heated wall) should far outweigh any increase of losses due to the elevation of the temperature of the unheated wall.

Another interesting observation in Fig. 2 is that separate bulk temperature lines have not been drawn for the with-radiation and without-radiation cases. The two lines are, in fact, coincident within the scale of the figure. This means that the radiation process, which has already been shown to be highly effective in transferring heat across the channel, does not transport significant amounts of energy along the channel. Further perspectives on this matter will be conveyed by the results for the first variant of the base case, which will now be discussed, and by the local heat flux results, to be presented later.

In the first variant of the base case, all parameter values listed in equation (21) are retained as before, but the length of the channel is reduced from $L/H = 200$ to $L/H = 100$. This variant was selected in order to examine whether the results for a long duct, such as for $L/H = 200$, can be employed for cases characterized by smaller L/H, merely by cutting off the curves at an x/H value equal to the L/H of interest.

As seen in Fig. 2, the wall and bulk temperature distributions for the $L/H = 100$ case are completely coincident with those for $L/H = 200$, except in a small region just upstream of $x/H = 100$ where the wall temperatures deviate slightly. Since the structure of the convective equations (3)–(5) does not permit upstream propagation of downstream effects, the slight deviation in evidence near $x/H = 100$ is due entirely to radiative exchange with the downstream plenum for the $L/H = 100$ case. The fact that the deviation is confined to the near neighborhood of $x/H = 100$ indicates that axial transport of energy by radiation is of no significance except near the plenums. It may also be concluded from Fig. 2 that wall and bulk temperature distributions for longer ducts can be truncated and used for shorter ducts.

For the second variant of the base case, the effect of

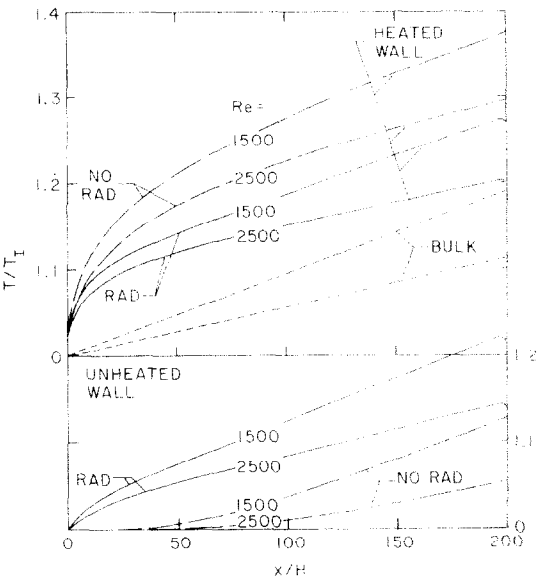

FIG. 3. Effect of Reynolds number on the wall and bulk temperature distributions.

Reynolds number will be considered. Correspondingly, all of the parameters of equation (21) retain their given values, but Re is decreased from 2500 to 1500. The wall and bulk temperature distributions for the variant and the base cases are presented in Fig. 3. Curves for the heated wall and for the bulk are plotted in the upper graph, while curves for the unheated wall are plotted in the lower graph.

The figure shows that the trends that were already identified for the higher Reynolds number (2500) also hold for the lower Reynolds number. However, careful inspection of Fig. 3 shows a greater reduction in the temperature of the heated wall at the lower Reynolds number and, concurrently, a greater increase in the temperature of the unheated wall. These findings can be rationalized by noting that the lower Reynolds number implies a lower value of the convective heat transfer coefficient,* which makes the direct transfer of heat from the hot wall to the fluid less easy. This causes the radiation path to appear relatively more attractive and enables radiation to be more effective in bringing the temperatures of the two walls closer together. At the downstream end of the passage, the higher temperatures attained in the lower Reynolds number case provide a further strengthening of the radiation owing to its fourth-power dependence on temperature.

Another interesting observation in Fig. 3 concerns the degree of thermal development for the pure convection case, as witnessed by the attainment or nonattainment of parallelism of the wall and bulk temperature lines. For $Re = 2500$, thermal development is not attained for the channel length $L/H = 200$, whereas development is attained when $Re = 1500$. In the presence of radiation, there is no evidence of parallelism of the bulk and wall temperature lines for either case.

* At all axial stations in the thermal development regime.

In the third variant of the base case, the trends associated with the parameter $\sigma T_I^3/(k/H)$ will be examined. This parameter is, in effect, a Nusselt number for radiation, with σT_I^3 playing the role of a heat transfer coefficient. To provide an unambiguous appraisal of the role of this parameter, it was deemed advisable to adjust $q_w/\sigma T_I^4$ as $\sigma T_I^3/(k/H)$ is varied, so that both the bulk temperature rise and the pure convection solution are unaffected by the changes. This is accomplished by holding $q_w{}^H T_I k$ constant. According to equation (12), constant values of this quantity can be attained by varying $\sigma T_I^3/(k/H)$ and $q_w/\sigma T_I^4$ in inverse proportions. Thus, if $\sigma T_I^3/(k/H)$ is increased from its base case value of 0.5 to 0.75, then $q_w/\sigma T_I^4$ has to be decreased from 1.0 to 2/3. The aforementioned changes have been made, and these define the third variant of the base case.

The wall and bulk temperature distributions for the just-defined variant and for the base case are compared in Fig. 4. As per design, the wall temperatures for pure convection are the same for the two cases, as are the bulk temperature distributions. When radiation participates, the temperature of the heated wall is shifted downward when $\sigma T_I^3/(k/H)$ is increased, and the temperature of the unheated wall is shifted upward. These shifts are consistent with a strengthened role of the radiative transfer, since it has already been established that radiation tends to bring the temperatures of the unheated and heated walls together. In addition, the shifts are consistent with the interpretation of $\sigma T_I^3/(k/H)$ as a Nusselt number for radiation, since increases in Nusselt number are generally indicative of a strengthening of the transport process represented by the Nusselt number.

Further examination of Fig. 4 shows that the shifts in the wall temperatures corresponding to a 50% increase in $\sigma T_I^3/(k/H)$ (from 0.5 to 0.75) are rather small. Therefore, substantially larger increases in this parameter are needed in order to induce significant changes in the wall temperatures.

The fourth and final variant to be considered is a reduction of the external heating parameter $q_w/\sigma T_I^4$ from 1.0 to 0.25, with all other parameters held fixed.

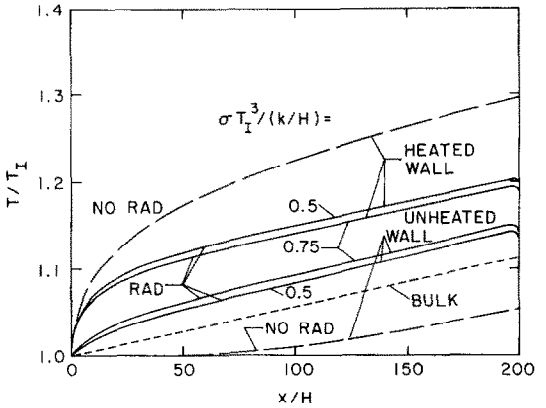

FIG. 4. Effect of the parameter $\sigma T_I^3/(k/H)$ on the wall and bulk temperature distributions.

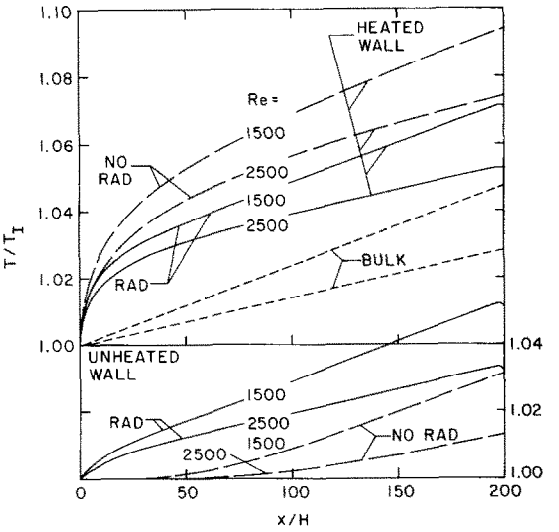

FIG. 5. Effect of the heating parameter $q_w/\sigma T_I^4$ on the wall and bulk temperature distributions.

Numerical solutions were carried out for the two previously considered Reynolds numbers, $Re = 2500$ and 1500, and the results are shown in Fig. 5. The structure of this figure is identical to that of Fig. 3, with the major difference being the substantial reduction in the range of the ordinate variable. It is this reduction in temperature level that is the main message of Fig. 5.

Along with the reduction in temperature level, the absolute effect of the radiative transfer also diminishes. However, radiation is by no means without effect. Thus, for example, the action of radiation raises the temperature of the unheated wall from values that are below the bulk temperature to values that are above the bulk temperature. Even with this, the radiation-induced wall temperature changes at relatively low external heat fluxes do not appear to be of great practical significance.

Wall heat flux distributions

To provide further perspectives about the role of radiation, distributions of the local convective heat fluxes on the heated and unheated walls are presented in Figs. 6 and 7, for $Re = 2500$ and 1500, respectively.

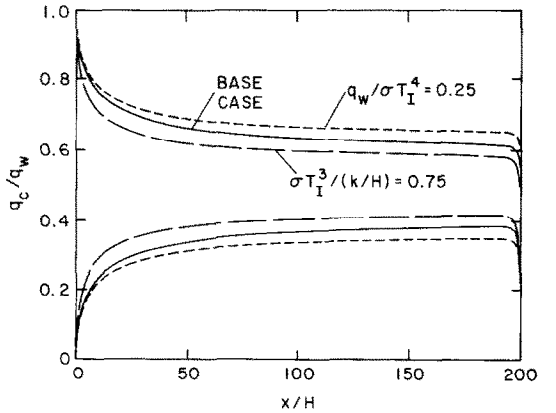

FIG. 6. Convective heat flux distributions, $Re = 2500$.

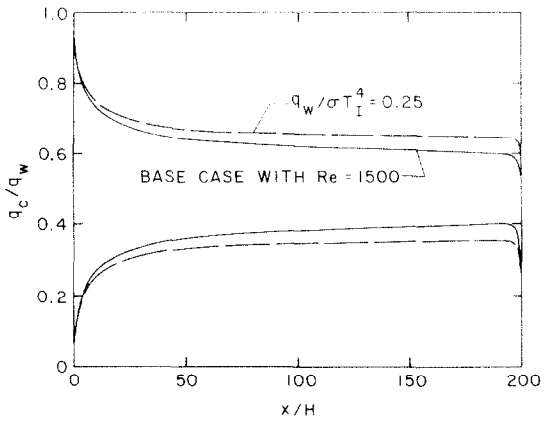

FIG. 7. Convective heat flux distributions, $Re = 1500$.

The ordinate is the ratio of the local convective flux q_c to the externally applied flux q_w. In each figure, the curves in the upper portion pertain to the heated wall, while those in the lower portion pertain to the unheated wall. To provide a backdrop for the discussion, it should be noted that for pure convection, the respective curves for the heated and unheated walls would be horizontal lines positioned at $q_c/q_w = 1$ and $q_c/q_w = 0$.

Inspection of the figures indicates a common trend for all cases. For the heated wall, $q_c/q_w \simeq 1$ at $x = 0$ and then decreases with increasing x, rather rapidly at first and then more gradually; in the neighborhood of the downstream plenum there is a sharp drop. The heat flux distributions for the unheated wall begin with q_c/q_w slightly greater than zero. Initially, the curves rise rapidly with x, with a more gradual increase at larger downstream distances. There is a rapid drop-off near the downstream plenum.

Perhaps the most interesting message of Figs. 6 and 7 is the magnitudes of q_c/q_w on the two walls. Over a large portion of the channel, say, for $x/H > 50$, $q_c/q_w \sim 0.6$–0.65 for the heated wall and $q_c/q_w \sim 0.35$–0.4 for the unheated wall. Thus, due to radiative transfer, the so-called unheated wall carries about 40% of the total convective heat load. Consequently, both walls are active participants in the convective transfer to the flowing fluid.

The curves appearing in each figure are arranged according to the relative strengths of the radiative transfer for the respective cases, as was discussed earlier in connection with Figs. 2–5. That discussion need not be repeated here. It is, however, relevant to explain the trend of the distributions with x. Near the inlet ($x = 0$), convection dominates because of the relatively high heat transfer coefficients associated with the initial thermal development of the flow. Consequently, heat flows readily from the heated wall to the fluid. As the thermal boundary layers grow with increasing downstream distance, the convection coefficients decrease. This weakening of the convection assists the radiation in its efforts to transport energy from the heated to the unheated wall. Correspondingly, the unheated wall takes on a greater share of the burden of heating the fluid, and the heated wall does less heating of the fluid.

Once the rapid changes in the convective coefficient have been completed, the q_c/q_w distributions tend to vary slowly, reflecting any residual changes in the convective coefficient as well as the increase in the temperature level (which tends to assist the radiation). Near the downstream plenum, the q_c/q_w values drop off rapidly owing to the net transfer of radiant energy from the duct walls to the plenum.

It is interesting to note that the q_c/q_w values for the heated and unheated walls sum to unity along the entire length of the channel, except near the ends. Near the inlet, the sum is slightly in excess of one, whereas at the exit the sum drops abruptly to about 0.75.

From a comparison of Figs. 6 and 7, it is seen that for corresponding cases (i.e. all parameters the same except for Re), the q_c/q_w values at the heated wall are higher at the larger Reynolds number, while the q_c/q_w values on the unheated wall are lower. This behavior is consistent with the already discussed lesser effectiveness of the radiative transfer at larger Reynolds numbers.

Nusselt number distributions

Local Nusselt numbers for the heated wall, evaluated from equation (20), are plotted in Figs. 8 and 9, respectively for $Re = 2500$ and $Re = 1500$. In addition to results for the radiation-affected cases, a curve for the pure convection case is included in each figure for reference purposes.

As expected, the high initial heat transfer coefficients drop off rapidly due to boundary layer development and then tend toward uniform or nearly uniform values in the downstream region. Whereas the radiation-affected coefficients do not differ appreciably from the pure convection values in the initial portion of the channel, substantial differences are in evidence in the downstream portion. In that region, the radiation-affected coefficients are about 25% higher than those for pure convection. The cause of the higher coef-

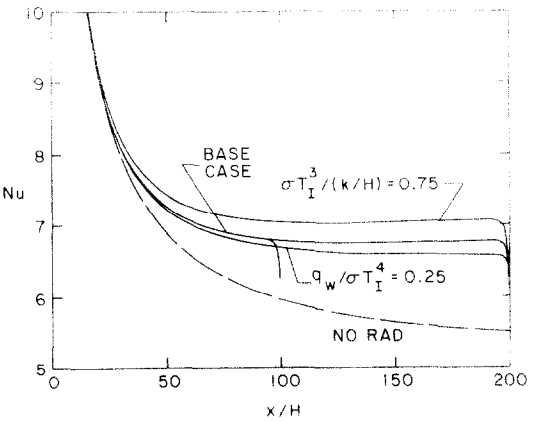

FIG. 8. Local Nusselt number distributions along the directly heated wall, $Re = 2500$.

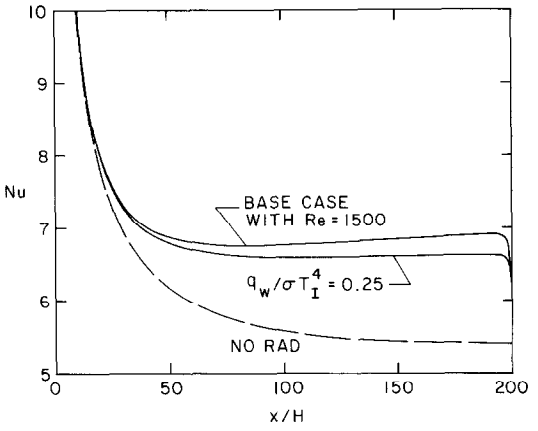

FIG. 9. Local Nusselt number distributions along the directly heated wall, $Re = 1500$.

ficients is the reduction in the wall temperature, resulting in lower values of $(T_w - T_b)$. This decrease in $(T_w - T_b)$ is greater than the reduction of q_c, with the result that $q_c/(T_w - T_b)$ increases due to radiation.

It is interesting to observe that the radiation-affected coefficients tend to level off at lower values of x/H than do the pure convection coefficients. Also, in some cases, notably the uppermost curve of Fig. 9, the radiation-affected coefficients tend to rise slightly in the downstream region. To explore the reason for this rise, the just-mentioned case (upper curve of Fig. 9) was re-run with $q_w/\sigma T_I^4 = 4$ rather than with $q_w/\sigma T_I^4 = 1$. This yielded a greater rise in Nu than that of Fig. 9. In addition, the higher heat flux brought forth higher temperature levels.

It is believed that the downstream rise in Nusselt number is intimately related to temperature level. At higher temperature levels, radiation becomes more effective in decreasing T_w. Since the highest temperatures and lowest convection coefficients are encountered in the downstream portion of the channel, increases in h due to decreases in $(T_w - T_b)$ appear plausible.

From a comparison of Figs. 8 and 9, it is evident that thermal development takes place more rapidly at lower Reynolds numbers, both with and without radiation participation. Immediately adjacent to the exit, the heat transfer coefficient drops sharply because of the sharp drop in q_c brought about by heat losses to the downstream plenum.

CONCLUDING REMARKS

The results presented here have demonstrated that radiative exchange in a channel can be highly effective in activating convective heat transfer to a flowing airstream from an otherwise unheated wall. In the case considered here, where one wall of the channel is externally heated and the other is externally adiabatic, the presence of the radiation causes the task of heating the fluid to be shared between the two walls. This sharing is most pronounced downstream of the initial portion of the thermal entrance region, where the high initial values of the heat transfer coefficient have given way to more moderate values. In the downstream region, for the cases studied here, about 60% of the external heat flux is transferred to the fluid at the directly heated plate and 40% is transferred at the radiatively heated plate.

The effect of the aforementioned sharing of the convective heating of the air is to reduce the temperature of the directly heated plate. This reduction has affirmative implications for the efficiency of an air-operated flat plate solar collector because the temperature decrease diminishes the heat losses through the cover system.

REFERENCES

1. G. O. G. Löf, personal communication (1979).
2. G. S. Beavers, E. M. Sparrow and R. A. Magnuson, Experiments on the breakdown of laminar flow in a parallel-plate channel, *Int. J. Heat Mass Transfer* **13**, 809–815 (1970).
3. E. G. Keshock and R. Siegel, Combined radiation and convection in an asymmetrically heated parallel plate channel, *J. Heat Transfer* **86C**, 341–350 (1964).
4. S. T. Liu and R. S. Thorsen, Combined forced convection and radiation in asymmetrically heated parallel plate channel, *Proceedings*, 1970 *Heat Transfer and Fluid Mechanics Institute*, pp. 32–44. Stanford University Press, Stanford, California (1970).
5. E. M. Sparrow and R. D. Cess, *Radiation Heat Transfer* (augmented edition). Hemisphere, Washington, D.C. (1978).
6. S. V. Patankar and D. B. Spalding, *Heat and Mass Transfer in Boundary Layers*, 2nd edn. Intertext Books, London (1970).
7. E. M. Sparrow, B. R. Baliga and S. V. Patankar, Heat transfer and fluid flow analysis of interrupted-wall channels, with application to heat exchangers, *J. Heat Transfer* **99C**, 4–11 (1977).

INTERACTION CONVECTION–RAYONNEMENT DANS UN CANAL A PLANS PARALLELES—APPLICATION AUX COLLECTEURS SOLAIRES A AIR

Résumé—L'analyse concerne le développement simultané des champs laminaires de vitesse et de température dans un canal à plans parallèles, avec intéraction de la convection et du rayonnement. Une paroi du canal est chauffée de l'extérieur alors que l'autre est isolée extérieurement ; l'air est le fluide de transfert. Ces conditions sont semblables à celles d'un collecteur solaire plan à air. Les résultats montrent que l'échange radiatif conduit le chauffage du fluide par convection à un partage entre les deux parois avec à peu près 40 pour cent du transfert par convection sur la paroi extérieurement adiabatique. Ceci peut conduire à une réduction sensible de la température du mur chauffé directement ce qui pour un collecteur solaire tend à augmenter son efficacité. Les nombres de Nusselt, en présence du rayonnement, sont plus élevés que ceux de la convection forcée pure.

WÄRMEAUSTAUSCH DURCH KONVEKTION UND STRAHLUNG ZWISCHEN PARALLELEN PLATTEN—ANWENDUNG AUF LUFTGEKÜHLTE SONNENKOLLEKTOREN

Zusammenfassung—Eine Untersuchung des Wärmetransports durch Konvektion und Strahlung zwischen zwei parallelen Platten für jeweils ausgebildetes laminares Geschwindigkeits- und Temperaturfeld wurde durchgeführt. Eine Wand des Strömungskanals wird von außen beheizt, die andere ist von außen isoliert. Wärmetransportmedium ist Luft. Die Bedingungen sind denen in einem luftgekühlten Sonnenflachkollektor ähnlich. Die Ergebnisse zeigen, daß der Strahlungsaustausch dazu führt, daß von beiden Wänden konvektiv Wärme an das Fluid übertragen wird, wobei ca. 40% des konvektiven Wärmestroms von der isolierten Wand übertragen werden. Hierdurch kann sich die Temperatur der direkt beheizten Wand merklich verkleinern, was für den Sonnenkollektor einen größeren Wirkungsgrad ergibt. Die Nusselt-Zahlen sind, wenn Wärmestrahlung vorhanden ist, größer als bei reiner erzwungener Konvektion.

ВЗАИМОДЕЙСТВИЕ МЕЖДУ КОНВЕКТИВНОЙ И ЛУЧИСТОЙ СОСТАВЛЯЮЩИМИ ТЕПЛООБМЕНА В ПЛОСКОПАРАЛЛЕЛЬНОМ КАНАЛЕ — ПРИЛОЖЕНИЕ К СОЛНЕЧНЫМ КОЛЛЕКТОРАМ С ВОЗДУШНЫМ ТЕПЛОНОСИТЕЛЕМ

Аннотация — Проведен анализ ламинарных полей скорости и температуры, развивающихся одновременно в плоскопараллельном канале, в котором происходит конвективный и лучистый теплоперенос. Одна из стенок канала нагревается снаружи, а другая теплоизолирована; теплоносителем служит воздух. Эти условия аналогичны тем, которые имеют место в пластинчатом солнечном коллекторе с воздухом в качестве теплоносителя. Результаты показывают, что из-за влияния лучистого переноса задача о конвективном переносе должна рассматриваться отдельно для каждой стенки, причем 40% конвективного переноса осуществляется вблизи адиабатической стенки. В результате может наблюдаться значительное снижение температуры непосредственно нагреваемой стенки, что приводит, в случае солнечного коллектора, к росту к. п. д. При учете лучистой составляющей значения числа Нуссельта выше значений, получаемых для одной вынужденной конвекции.